IUST
Iran University of Science and Technology

Iranian Journal of Electrical and Electronic Engineering

Journal Homepage: ijeee.iust.ac.ir

Research Paper

An Improved Transformerless Grid-Connected PV System With Related Control Strategy to Reduce Leakage Current, Extract Maximum Power Point and Control Power

T. Ahmadzadeh*, E. Babaei**(C.A.), M. Sabahi**, and T. Abedinzadeh*

Abstract: The main purposes of a transformerless grid-connected photovoltaic (PV) system consist of the reduction of leakage current, extraction of maximum power point (MPP), tracking of MPP (MPPT), controlling the active and reactive powers, and having the unity power factor. To achieve the above-mentioned aims, the following actions have been performed in this paper. First of all, a brief analysis of the transformerless PV system has been done by using the conventional full-bridge (FB) topologies with two bipolar and unipolar PWM techniques. Then, an effective solution has been also introduced to significantly reduce the leakage current in the conventional H5 FB topology. Moreover, a proper control method has been proposed by using the combination of the fractional open-circuit voltage (FOCV) and the model predictive control (MPC) strategies to extract the MPP from PV panels, control the injection of the reactive power to the gird and have the unity power factor. At last, the simulation results performed in PSCAD software will be used to prove the correct performance of the proposed control method in the improved H5 FB topology.

Keywords: Full Bridge (FB) Inverter, H5 FB Topologies, Leakage Current, Pulse Width Modulation (PWM) Techniques, Bipolar PWM (BPWM) Modulation, Unipolar PWM (UPWM) Modulation, Maximum Power Point (MPP) Tracking, Fractional Open-Circuit Voltage (FOCV) Technique, Model Predictive Control (MPC) Strategy.

1 Introduction

PHOTOVOLTAIC (PV) systems are mainly categorized as stand-alone and grid-connected systems. The stand-alone system directly supplies the power to a load or an electrical appliance. While the grid-connected systems not only supply the power to a load or an electrical appliance but also inject the power into the grid [1-3].

Iranian Journal of Electrical and Electronic Engineering, 2020.
Paper first received 20 June 2019, revised 01 October 2019, and accepted 04 October 2019.
* The authors are with the Department of Electrical Engineering, Shabestar Branch, Islamic Azad University, Shabestar, Iran.
E-mails: t-ahmadzadeh@iaushab.ac.ir and taherabedinzade@iaushab.ac.ir.
** The authors are with the Faculty of Electrical and Computer Engineering, University of Tabriz, Tabriz, Iran.
E-mails: e-babaei@tabrizu.ac.ir and sabahi@tabrizu.ac.ir.
Corresponding Author: E. Babaei.

The grid-connected PV systems have various topologies by applying the interface converters. These converters can consist of single- or two-stage topologies [4-9]. The single-stage topology uses only one inverter in order to convert the DC-voltage to an AC-voltage and control the duty cycle of the inverter for extracting the maximum power point (MPP) from the PV panels [2], [4-6]. Whereas the two-stage topology applies two converters such as DC-DC and DC-AC (or inverter). In this topology, the DC-DC converter has been used to extract the MPP from the PV panels by controlling the duty cycle of the DC-DC converter. While an inverter has been used to convert the DC-voltage to an AC-voltage and inject the active power into the grid by controlling the duty cycle of the inverter [5, 8, 9]. The two-stage structure compared to the single-stage one will have a good performance in terms of the MPP tracking (MPPT), but the total efficiency of the system can be decreased because of the presence of two converters [4, 5].

On the other hand, the PV systems are also categorized as transformer and non-transformer structures. The transformer topology in comparison with the non-transformer topology can increase the safety and reliability of the system, but the total efficiency of the system will be decreased and the volume, weight, and cost of the system will be increased [10-13].

It should be noted that one of the differences between the inverters used in renewable applications (such as PV, wind turbine, and FC systems) and the conventional inverters is that the input voltage of H-bridge is variable in the renewable systems. Therefore, the input power density of the inverters used in renewable applications should be able to handle a variable power density, which requires high efficiency over a wide range. If the inverter used in them is non-transformer topology, the efficiency will be high because the efficiency factor of the transformer does not apply to the total system efficiency. Nevertheless, the non-transformer topologies are less commonly used in practical applications in order to the safety and reliability issues [1, 11, 12]. It is noticeable that the necessary condition for the injection of active power from the PV panel to the power grid is having a voltage level higher than the grid voltage. Hence, one of the fundamental problems in non-transformer structures is the need for a high voltage level in the PV panels, which will also increase the leakage currents of the PV panels. Increasing the leakage current also reduces the safety and reliability of the system [1, 3, 12]. Moreover, the dispersed capacities generated by the PV panel, especially in the rainy and polluted air, lead to flow a leakage current toward the ground. So that the protective fuses used in the system can be acted and the system will be cut-off.

Up to now, various topologies for a grid-connected PV system based on non-transformer have been introduced [11], [14-17]. Some of these topologies are the conventional FB (H4) inverter, the H5 from SMA Corporation, the H6 FB inverters, the HERIC topology from Sunways Company, FB inverter with DC bypass, high-efficiency inverter with H6-type configuration, and single-phase three-level diode-clamped inverter [14], [16-21].

One of the main issues in the transformerless PV systems which should be noted is the reduction of leakage current toward the ground [14-16]. To overcome this problem, an efficient topology or a suitable PWM control method can be used [22]. Another fundamental issue in these systems is the extraction of MPP from the PV panels which can be achieved by using the maximum power point tracking (MPPT) control algorithms such as perturb and observe (P&O), incremental conductance (IncCond), fractional Open-Circuit Voltage (fractional V_{oc}), fractional Short-Circuit Current (fractional I_{sc}), fuzzy logic control, neural networks [23-26]. Other important subjects in the transformerless PV systems consist of controlling the active and reactive powers and achieving the unity power factor [20-22].

To obtain the above-mentioned issues, this paper is categorized as follows. In Section 2, a brief review of the operating principle of a grid-connected PV system based on the transformerless topology has been analyzed by using the conventional single-phase FB and H5 FB structures. In Section 3, an improved structure is presented for the conventional H5 FB inverter due to a reduction in the ground leakage current. By using the combination of the FOCV and the model predictive control (MPC) strategies, a suitable control method is proposed to achieve the MPP, less injection reactive power to the gird and unity power factor. In Section 4, the perfect function of the proposed control method with the related equations is presented. To demonstrate the analysis validity for the transformerless grid-connected PV system based on improved H5 FB topology with the related controller, the simulation results are provided in Section 5.

2 Review of the Conventional Transformerless PV Systems Based on Full Bridge Topologies

Fig. 1 shows a transformerless grid-connected PV system by using the conventional single-phase FB inverter. In Fig. 1, the DC-link capacitor (C_{PV}) is used to stabilize the input voltage of the PV array and create a smooth DC current at the input of H-bridge. To convert the PWM waveform to a sinusoidal waveform in the output of H-bridge, an inductor's filter (L_f) is applied. Since the generated oscillations in the voltage of the grid side are almost constant, a voltage stabilizer capacitor (C_{Fix}) will be also used. Considering Fig. 1, the ground leakage current (the common-mode current) flows in each of phase legs because of the variations in the common-mode voltage (v_{cm}) [1, 3]. In order to the reduction of ground leakage current, the voltage across the capacitor (common-mode voltage) should be kept in a constant value [27]. Hence, the value of the common-mode voltage (v_{cm}) can be calculated as follows:

$$v_{cm} = \frac{v_{an} + v_{bn}}{2} \tag{1}$$

where v_{an} and v_{bn} are the output voltages for each of phase legs, respectively.

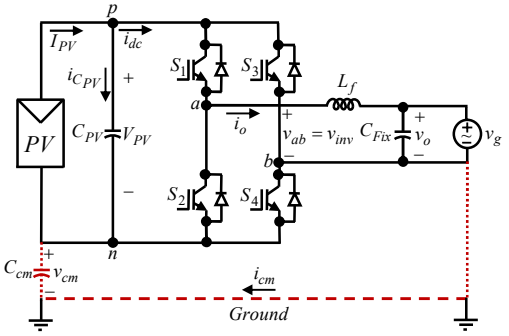

Fig. 1 The transformerless grid-connected PV system by using the single-phase FB inverter [1, 27].

To control the switches of the FB inverter, various methods are available which one of them is the bipolar PWM (BPWM) modulation technique that is shown in Fig. 2. According to Figs. 1 and 2, if these switches have been switched by using the BPWM technique, the results at the first and second operation modes are respectively equal to (2) and (3) as follows:

$$\begin{cases} v_{an} = v_{S2} = V_{PV} \\ v_{bn} = v_{S4} = 0 \end{cases} \Rightarrow v_{cm} = \frac{V_{PV}}{2} \quad \text{for} \quad S_1 \,\&\, S_4 : ON \tag{2}$$

$$\begin{cases} v_{an} = v_{S2} = 0 \\ v_{bn} = v_{S4} = V_{PV} \end{cases} \Rightarrow v_{cm} = \frac{V_{PV}}{2} \quad \text{for} \quad S_2 \,\&\, S_3 : ON \tag{3}$$

According to (2) and (3), in the steady-state, the values of common-mode voltage are constant for two operation modes and the leakage current will be much lower. In the BPWM, not only whole switches are switched in low frequency (grid frequency) but also the zero states are not generated. However, due to the high switching losses and high current ripple, this switching method cannot be used in practice. To solve the BPWM problems, the unipolar PWM (UPWM) technique can be used. There are different strategies to control the switches of the FB inverter which are shown in Fig. 3. Considering the first technique shown in Fig. 3(a), nevertheless the zero states are generated but due to the switching of all switches in high frequency (switching frequency), an increase in switching losses will be caused. Hence, it cannot be suitable in practice. In the second UPWM technique shown in Fig. 3(b), opposite of the first technique, two switches (S_1 and S_2) are switched in grid frequency whereas the other two (S_3 and S_4) are switched in switching frequency which causes a reduction in the switching losses. In this method, two operating modes can occur for the positive and negative half-cycles. Considering Fig. 3(b), the values of the common-mode voltage are different from zero to V_{PV}, which causes an increase in the leakage current. Nevertheless, a reduction in the current ripple of the L_f inductor has happened because of generating the zero voltage. To solve this problem, the other two UPWM techniques will be applied as shown in Figs. 3(c) and 3(d). These strategies reduce the alteration of v_{cm} value from $V_{PV}/2$ to V_{PV} in the third technique (Fig. 3(c)) and from zero to $V_{PV}/2$ in the fourth one (Fig. 3(d)).

To overcome the problems of PWM control methods for the FB structure, the non-transformer topology such as H5 FB topology can be used which is shown in Fig. 4. Table 1 shows the different combinations of allowed switching states for switches of the H5 FB inverter. In Table 1, v_{ab} is the output voltage of the inverter. Considering Fig. 4 and Table 1, by using the third UPWM technique, the switches of the H5 FB inverter have three operating modes; which generate three levels of voltage ($-V_{PV}$, 0, $+V_{PV}$) in the output of the inverter. The switch of S_5 is turned on when the

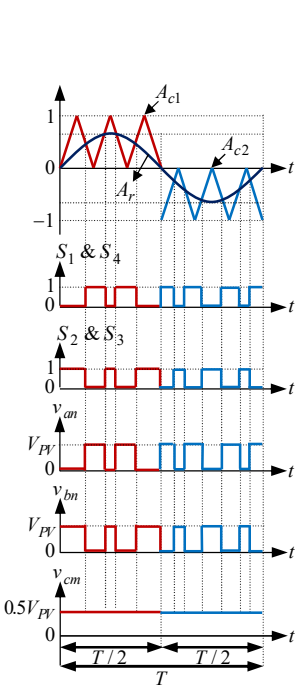

Fig. 2 The BPWM modulation strategy for the FB inverter.

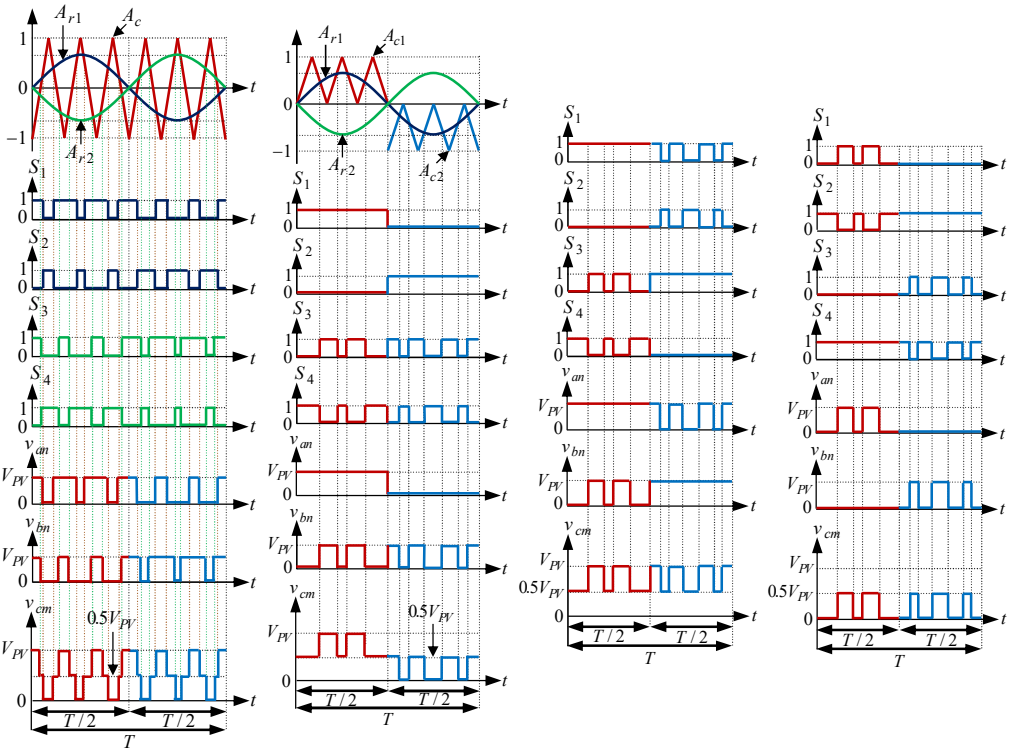

Fig. 3 The UPWM modulation strategies for the FB inverter: a) First technique, b) Second technique, c) Third technique, and d) Fourth technique.

output voltage of the inverter ($v_{ab} = v_{inv}$) is equal to $+V_{PV}$ or $-V_{PV}$. So, we can write:

$$\begin{cases} v_{an} = V_{PV} \\ v_{bn} = 0 \end{cases} \Rightarrow v_{cm} = \frac{V_{PV}}{2} \quad \text{for} \quad \begin{cases} S_1 \,\&\, S_4 : ON \\ S_5 : ON \end{cases} \tag{4}$$

$$\begin{cases} v_{an} = 0 \\ v_{bn} = V_{PV} \end{cases} \Rightarrow v_{cm} = \frac{V_{PV}}{2} \quad \text{for} \quad \begin{cases} S_2 \,\&\, S_3 : ON \\ S_5 : ON \end{cases} \tag{5}$$

It is noticeable that in the positive and negative half-periods, the switch of S_5 is switched respectively in the switching and grid frequencies. According to Fig. 4, to calculate the zero voltage in the output H5 inverter at the positive and negative half-periods, we can write:

$$\begin{cases} v_{an} = v_{S2} = V_{PV} - v_{S5} \\ v_{bn} = v_{S4} = V_{PV} - v_{S5} \end{cases} \Rightarrow \text{for} \quad \begin{cases} S_1 \,\&\, S_3 : ON \\ S_5 : OFF \end{cases} \tag{6}$$

Considering (6), if the division of the input source voltage among S_2, S_4, and S_5 switches has been correctly done, the values of v_{an} and v_{bn} will be equal to $V_{PV}/2$, which the $v_{cm} = V_{PV}/2$. But due to the presence of the non-ideal commutations and parasitic capacitors and inductances, the voltage across the S_5 switch is almost equal to $2V_{PV}/3$ whereas it is $V_{PV}/3$ for S_2 and S_4 switches. Hence, the values of the common-mode voltage for positive half-period can be obtained as follows:

$$\begin{cases} v_{an} \approx \frac{V_{PV}}{3} \\ v_{bn} \approx \frac{V_{PV}}{3} \end{cases} \Rightarrow v_{cm} \approx \frac{V_{PV}}{3} \quad \text{for} \quad \begin{cases} S_1 \,\&\, S_3 : ON \\ S_5 : OFF \end{cases} \tag{7}$$

From (4) to (7), it can be concluded that the amplitude variation of v_{cm} will be between $V_{PV}/3$ and $V_{PV}/2$ in the positive and negative half-periods, which has been also proved in the simulation results. Hence, the ground leakage current will be increased.

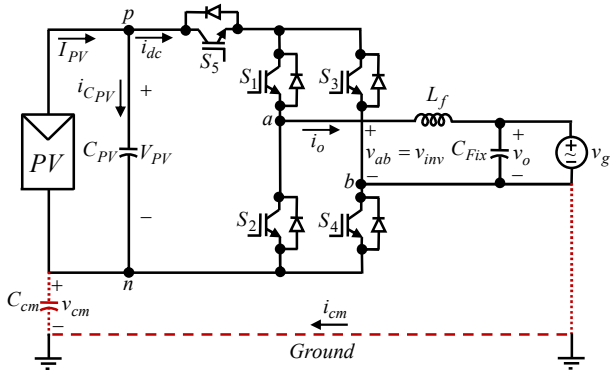

Fig. 4 The transformerless grid-connected PV system by using the single-phase based on H5 FB inverter [1, 27].

Table 1 The permissible switching states for switches of the single-phase H5 FB inverter.

Allowed switching states					v_{ab}
S_1	S_2	S_3	S_4	S_5	
ON	OFF	OFF	ON	ON	$+V_{PV}$
ON	OFF	ON	OFF	OFF	0
OFF	ON	ON	OFF	ON	$-V_{PV}$

3 Improved Topology

The conventional H5 FB inverter for producing zero voltage states at positive and negative half-periods has various values for the common-mode voltage [1, 27]. To overcome this problem, an effective solution is introduced in this paper which causes much more reduction in the ground leakage current. Fig. 5 shows the improved H5 FB topology. This topology uses an extra diode in the DC-link side to eliminate the variation of v_{cm} at two half-periods. Considering Table 1, the permissible switching states with the values of v_{an}, $v_{bn,}$ and v_{cm} for the conventional and improved H5 FB topologies by using the UPWM strategy are shown in Fig. 6. According to Figs. 5 and 6(b), it can be seen that the value of the common-mode voltage at one cycle is fixed ($v_{cm} = V_{PV}/2$) due to the addition of an extra diode in the improved topology. It should be noted that to generate the zero voltage at two half-cycles, the switch of S_5 is turned off whereas the diode of D is turned on. Hence, the values of v_{an} and v_{bn} are equal to $V_{PV}/2$ which causes a constant value for v_{cm}. On the other hand, the voltage across the S_5 switch is limited to $V_{PV}/2$ in the improved topology.

As shown in Fig 6, the voltage across the capacitor (common-mode voltage) in the improved topology has been kept at the constant value ($v_{cm} = V_{PV}/2$), whereas it is variable from $V_{PV}/3$ to $V_{PV}/2$ in the conventional H5 FB topology [1, 27]. So, not only the ground leakage current has been significantly reduced in the improved topology due to the existence of D diode, but also the safety and reliability of the system are increased due to the presence of S_5 switch (isolation issue).

4 Proposed Control Method Based on the Combination of the FOCV and MPC Strategies

Fig. 7 shows a general block diagram of the improved grid-connected PV systems with the proposed control method by exploiting the FOCV and MPC strategies. To

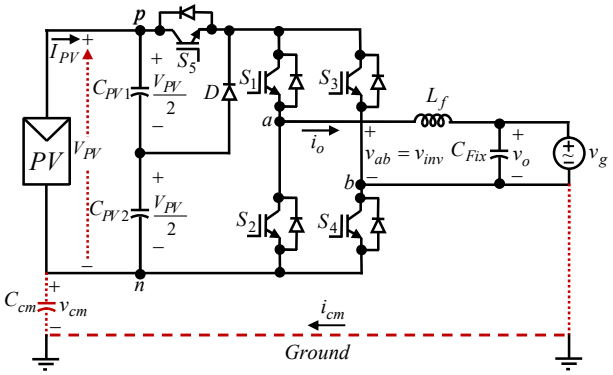

Fig. 5 The improved topology of the H5 FB inverter.

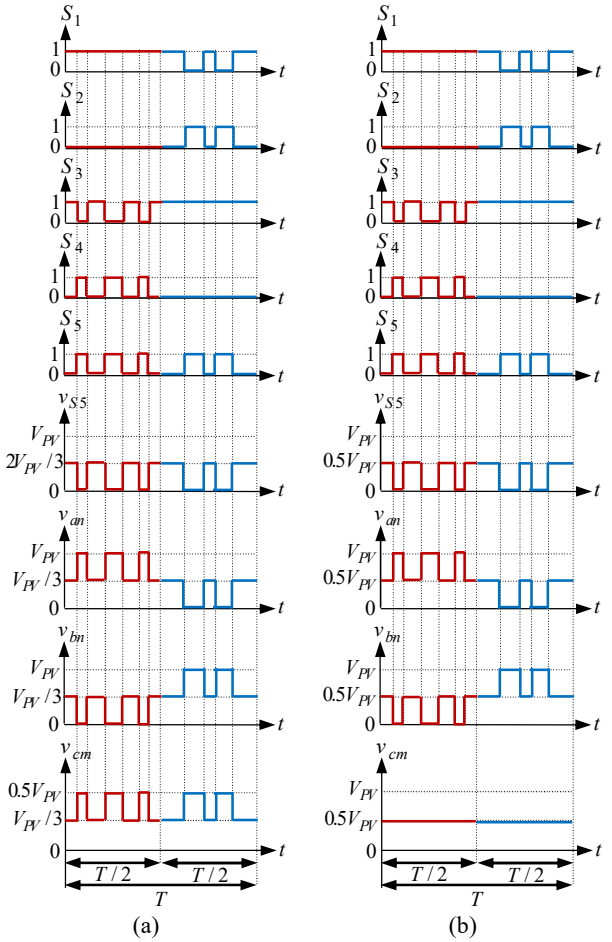

Fig. 5 The UPWM strategy: a) For the conventional H5 FB inverter and b) For the improved H5 FB inverter.

trace the MPP of the PV panel at any time, the voltage and current values of the PV panels are needed which can be achieved by two voltage and current sensors. The output of the MPPT block indicates the direction of motion. In some advanced MPPT methods, the value of motion direction can also be given. Since the MPP algorithm provides the best work point for values of $V^*_{PV} = V_{MPP}$ and $I^*_{PV} = I_{MPP}$, the value of MPP can be calculated by the equation of $P_{PV} = V^*_{PV} \times I^*_{PV} = V_{MPP} \times I_{MPP}$. Due to the existence of the losses in the inverter, the values of the input and output powers are not equal to each other. Hence, the inverter efficiency (η_{inv}) should be considered in calculating the value of the output power.

$$P_{o,inv} = \eta_{inv} \times P_{i,inv} = \eta_{inv} \times P_{MPP} = \eta_{inv} (V_{MPP} \times I_{MPP}) \quad (8)$$

where $P_{i,inv}$ and $P_{o,inv}$ are the input and output powers of the inverter, respectively.

Another point in the design of interface inverters is that the input current ripple of the inverter must be attempted to be close to the zero ($\Delta i_{dc} \rightarrow 0$), because the high ripple of the inverter input current causes the reduction of PV panel efficiency. In other words, in spite of achieving the MPP, the current ripple leads to the power losses and MPP will fluctuate around the optimal work point. To overcome this problem, a filter of the inductor and capacitor (LC filter) is used for the input of advanced inverters in renewable energy applications. But the inductor is eliminated in simpler inverters and only a large capacitor is used (Fig. 5). The used capacitor in the input of the inverter will act as an integrator. The input current ripple of the inverter can be smoother when the capacity of a capacitor has been increased. Moreover, the voltage across the C_{Fix} capacitor (v_o) is a sinusoidal waveform with the amplitude of V_m. It is necessary to explain that the phase difference between the voltage of v_o and network voltage (v_g) is very little (almost 1 to 2 degrees). Thus, the phase of them will be approximately the same.

In this paper, to extract the MPP from the PV panels, the FOCV (fractional V_{OC}) algorithm will be applied. This algorithm is one of the simplest and easiest techniques for MPP tracking. The operation principle of the FOCV technique is based on multiplying the open-circuit voltage of the panel at a constant value ($V_{MPP} \approx a V_{oc}$), in which the value of a can be deferent among 0.71 to 0.78 by considering the characteristic of PV array [23-26].

Moreover, the purpose of selecting the MPC control method in this paper is controlling the active and reactive powers and achieving the unity power factor. In the MPC algorithm, a sine reference current ($i_{o,ref}$) with the amplitude of $I_{m,ref}$ (which is determined by the controller) is firstly defined. Then, the control circuit will be designed in order that the inverter output current (i_o) be able to track the reference current. The operation principle of the MPC control strategy is shown in Fig. 8. Since the reference current is a sinusoidal waveform, it has a lower total harmonic distortion (THD).

In addition, because the phase of this current is as same as the grid voltage phase, the reactive power injection into the grid will be approximately equal to zero ($Q \approx 0$). By assuming that the i_o is able to track the $i_{o,ref}$, the average injunction power ($P_{o,ave}$) can be calculated as follows:

$$\begin{aligned} P_{o,ave}(\omega t) &= \frac{1}{2\pi}\int_0^{2\pi} v_o(\omega t)\, i_{o,ref}(\omega t)\, d\,\omega t \\ &= \frac{1}{2\pi}\int_0^{2\pi} (V_m \sin\omega t)(I_{m,ref} \sin\omega t)\, dt \\ &= \frac{V_m \times I_{m,ref}}{2} \end{aligned} \quad (9)$$

In (9), the amplitude of reference current ($I_{m,ref}$) is unknown. Therefore, by considering the relations obtained from (8) and (9), we will have:

$$P_{o,ave} = P_{o,inv} \Rightarrow \frac{V_m \times I_{m,ref}}{2} = \eta_{inv} (V_{MPP} \times I_{MPP}) \quad (10)$$

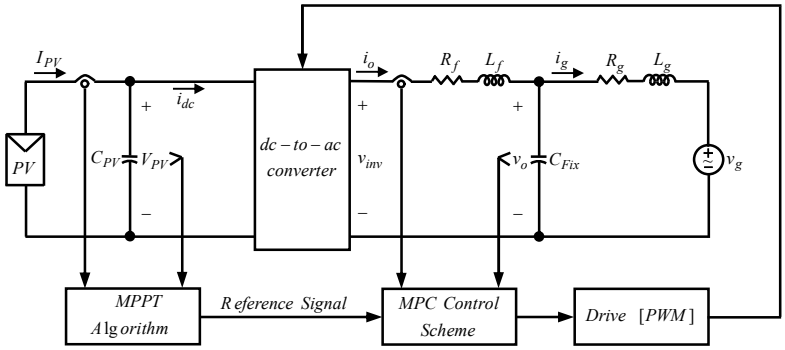

Fig. 7 Block diagram of a grid-connected PV system with the proposed control method based on FOCV and MPC algorithms.

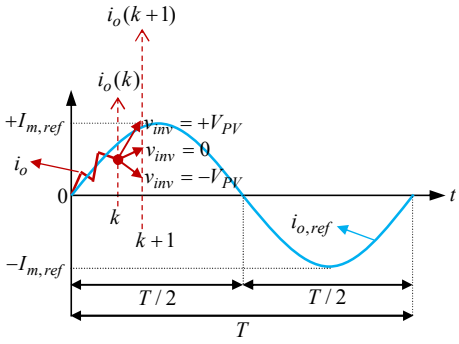

Fig. 8 The MPC control strategy.

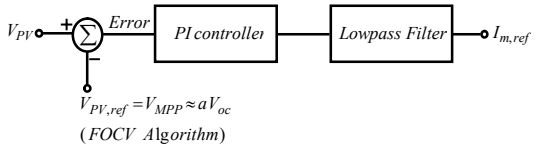

Fig. 9 The generation process of the reference current amplitude.

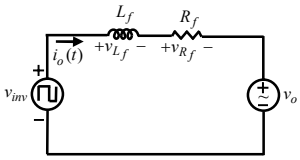

Fig. 10 The simplified equivalent circuit for Figs. 1, 4, and 5.

From (10), $I_{m,ref}$ is equal to:

$$I_{m,ref} = \frac{2\eta_{inv}(V_{MPP} \times I_{MPP})}{V_m} \quad (11)$$

In the proposed control method, to generate the amplitude of sine reference current ($I_{m,ref}$), the following processes will be performed. First, the PV voltage generated by the PV panel (V_{PV}) will be compared with the PV reference voltage ($V_{PV,ref} = V_{MPP}$) which is achieved by applying the FOCV algorithm. Then, the obtained result of the comparison should be given to the input of a PI controller. Finally, the PI controller output will apply to the input of a low-pass filter. The obtained result of the output of the low-pass filter will generate the optimum value of $I_{m,ref}$. Fig. 9 shows the generation process of the amplitude of the reference current. Fig. 10 shows the simplified equivalent circuit for Figs. 1, 4, and 5. Considering this figure, the output voltage of the inverter ($v_{ab} = v_{inv}$) can have three values which are $-V_{PV}$, 0, and $+V_{PV}$ (Fig. 8).

By writing the voltage law of Kirchhoff for the equivalent circuit shown in Fig. 9, we will have:

$$v_{inv} = L_f \frac{di_o}{dt} + R_f i_o + v_o \cong L_f \frac{\Delta i_o}{\Delta t} + R_f i_o + v_o \quad (12)$$

Considering Fig. 7, (12) can be rewritten for the time of $t = k$:

$$v_{inv}(k) = \frac{L_f}{T}\left[i_o(k+1) - i_o(k)\right] + R_f i_o(k) + v_o(k) \quad (13)$$

where T is the decision-making period and $f = 1/T$ is the decision-making frequency. Also, $i_o(k+1)$ is the estimated current in the next step.

Since the voltage variation across the stabilizer capacitor (ΔV_{CFix}) is very little for the steps of $t = k$ and $t = k+1$, the value of $v_o(k)$ will be approximately equal to the value of $v_o(k+1)$.

From (13), the estimated current of $i_o(k+1)$ can be calculated as follows:

$$i_o(k+1) = \frac{T}{L_f}\left[v_{inv}(k) - R_f i_o(k) - v_o(k)\right] + i_o(k) \quad (14)$$

According to Fig. 8 and (14), in time of $t = k+1$, the three values of $-V_{PV}$, 0 and $+V_{PV}$ can be selected for the output voltage of the inverter. Thus, the estimated current of $i_o(k+1)$ is compared with the reference current of $i_{o,ref}(k+1)$ for all three values of $-V_{PV}$, 0, and $+V_{PV}$, in the first place. So we have:

$$\varepsilon_1 = \left| i_o(k+1)\big|_{v_{inv}=+V_{PV}} - i_{o,ref}(k+1) \right|$$
$$\varepsilon_2 = \left| i_o(k+1)\big|_{v_{inv}=0} - i_{o,ref}(k+1) \right|$$
$$\varepsilon_3 = \left| i_o(k+1)\big|_{v_{inv}=-V_{PV}} - i_{o,ref}(k+1) \right| \quad (15)$$

Then, the smallest obtained value for the estimated current of $i_o(k+1)$ is chosen as the closest one to the reference current of $i_{o,ref}(k+1)$. So we can write:

$$\varepsilon_{select} = \min\{\varepsilon_1, \varepsilon_2, \varepsilon_3\} \quad \Rightarrow \quad i_o(k+1)\big|_{\varepsilon_{select}} \quad (16)$$

It should be noted that the controller circuit has been applied at discontinuous times which means in each certain intervals of time, an interruption interval is considered for the control circuit. So that the controller circuit checks the existing conditions at different moments (such as $t = 0$, $t = k\text{-}1$, $t = k$, $t = k\text{+}1$, etc.) and at last a decision-making process will be performed. Considering (12) to (16) and Fig. 8, the value of i_o is equal to zero in $t = 0$ and besides for tracking of the $i_{o,ref}$, the S_1 and S_4 switches must be turned on. In other words, to produce a positive current, the output voltage of the inverter should be a positive value. Moreover, the value of i_o is smaller than the value of $i_{o,ref}$ in the time of $t = k$ (Fig. 8). Hence, the S_1 and S_4 switches are also turned on to track the $i_{o,ref}$. While at the time of $t = k\text{-}1$, the value of i_o is greater than the value of $i_{o,ref}$. Thus, to track the $i_{o,ref}$ by i_o, either the S_2 and S_3 switches (which means the production of a negative voltage) or the S_1 and S_3 switches (which means the production of a zero voltage) must be turned on. As a result, the main advantages of the MPC technique are the selection of switching with the lowest losses, the proper tracking of sine reference current by the inverter output current and controlling the active and reactive powers. It is noticeable that, in the proposed control method based on FOCV and MPC, to obtain the value of MPP can be also simply used the other of more exact algorithms for MPPT because it creates not only any limitation and interference but also it can increase the accuracy of the control method.

5 Simulation Results

To validate the system performance, the simulation is performed in the PSCAD software. The used parameters in the simulation are shown in Table 2. The simulation results for different conditions of the sun's radiation intensity and environment temperature are shown in Figs. 11 to 16.

Figs. 11 and 12 show the operating principle of the conventional and improved H5 FB inverters by using the UPWM strategy shown in Fig. 6, respectively. In the conventional H5 topology, the value of the common-mode voltage at positive half-period due to (4) and (7) will be equal to:

$$v_{inv} = +V_{PV} : \begin{cases} v_{an} = V_{PV} \\ v_{bn} = 0 \end{cases} \Rightarrow v_{cm} = \frac{V_{PV}}{2} = \frac{330^{V}}{2} = 165^{V}$$

$$v_{inv} = 0 : \begin{cases} v_{an} \approx \frac{V_{PV}}{3} \\ v_{bn} \approx \frac{V_{PV}}{3} \end{cases} \Rightarrow v_{cm} \approx \frac{V_{PV}}{3} = \frac{330^{V}}{3} = 110^{V}$$

In the following, at negative half-period, the value of v_{cm} considering (6) and (7) will be equal to:

$$v_{inv} = -V_{PV} : \begin{cases} v_{an} = 0 \\ v_{bn} = V_{PV} \end{cases} \Rightarrow v_{cm} = \frac{V_{PV}}{2} = \frac{330^{V}}{2} = 165^{V}$$

$$v_{inv} = 0 : \begin{cases} v_{an} \approx \frac{V_{PV}}{3} \\ v_{bn} \approx \frac{V_{PV}}{3} \end{cases} \Rightarrow v_{cm} \approx \frac{V_{PV}}{3} = \frac{330^{V}}{3} = 110^{V}$$

Table 2 Used parameters in the simulation.

Open-circuit voltage	V_{oc}	450 V
Short-circuit current	I_{sc}	8 A
Factor of the FOCV	a	0.74
DC-Link capacitor	C_{PV}	3300 µF
Output filter values	R_F	0.1 Ω
	L_F	15 mH
Stabilizer capacitance values	C_{Fix}	0.1 µF
	R_{Fix}	0.1 Ω
Grid impedance	R_g	0.1 Ω
	L_g	1 mH
Grid voltage amplitude	V_m	310 V
Grid frequency	f_g	50 Hz
Decision frequency	f	10 Hz

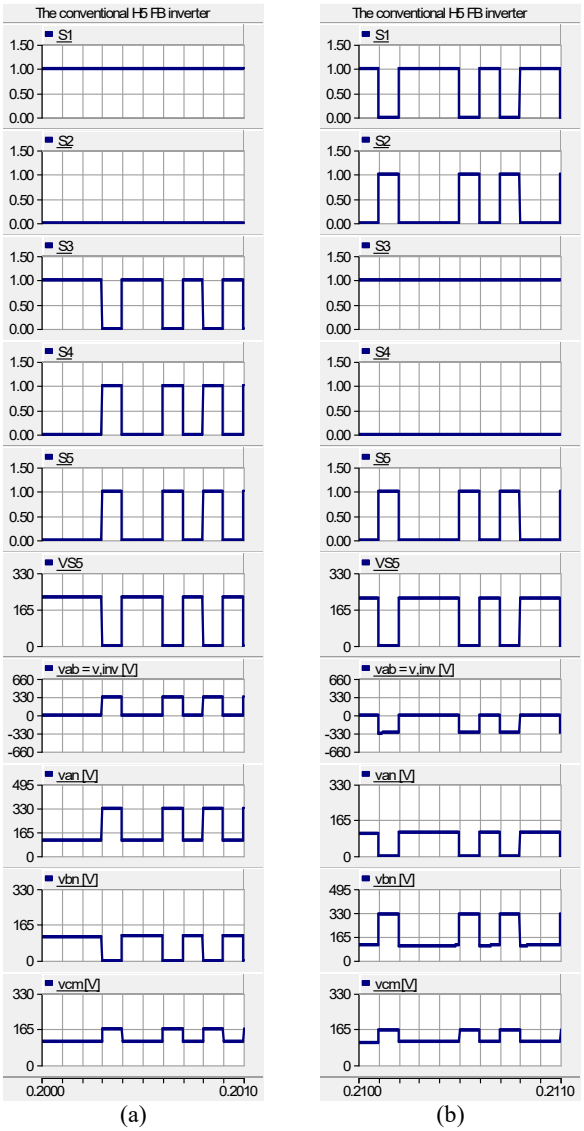

(a) (b)

Fig. 11 The UPWM technique for the conventional H5 FB inverter: a) A part of positive half-period and b) A part of negative half-period.

Considering the four equations above and Figs. 6(a) and 11, the amplitude variation of v_{cm} is between $V_{PV}/3$ and $V_{PV}/2$ at the positive and negative half-periods for the conventional H5 FB topology. Whereas, it is constant and equal to $V_{PV}/2$ for the improved topology which is shown in Figs. 6(b) and 12.

As a result, the obtained simulation results in 12 prove that the improved H5 topology has constant variation in one cycle, which means having more lower leakage current. On the other hand, the voltage across the S_5 switch is limited to $V_{PV}/2$ in the improved topology, whereas it is $2V_{PV}/3$ in the conventional topology (Fig. 11).

Fig. 13 shows the harmonic contents for the conventional and improved H5 FB inverters. The harmonic components have been decreased in the improved topology (Fig. 13 (b)).

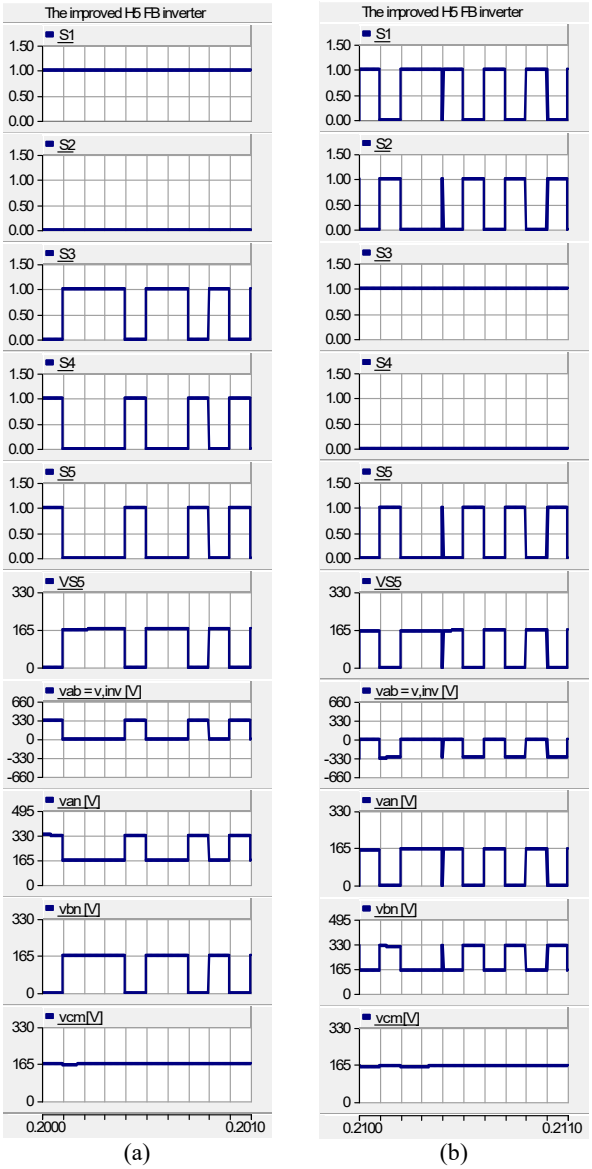

(a) (b)

Fig. 12 The UPWM technique for the improved H5 FB inverter: a) A part of positive half-period and b) A part of negative half-period.

Figs. 14 to 16 verify the correctness principle of the proposed control method based on the combination of the FOCV and MPC techniques for the improved H5 FB topology. During the time intervals of simulation, the solar radiation is variable from 600 W/m^2 to 1000 W/m^2, and the environment temperature differs from 20°C to 40°C. Fig. 14 shows the characteristic curve of the PV panel voltage in terms of the PV panel power (V_{PV}–P_{PV}) under different conditions of solar radiations and temperatures. Fig. 15 has been presented to analyze the operation of the FOCV algorithm by MPP extraction from the PV panel under different situations of weather. To prove this issue, the voltage of the PV panel (V_{PV}) should be able to track the PV reference voltage ($V_{PV,ref}$) besides the decreasing and increasing of values of $V_{PV,ref}$. According to Figs. 14 and 15, it has been observed that notwithstanding the alteration of weather conditions, the MPP point changes from 1.5 to 2.5 kW, which demonstrates the correct performance of the FOCV algorithm.

The main purpose of the MPC technique is controlling the active and reactive powers and achieving the unity power factor by proper tracking of reference

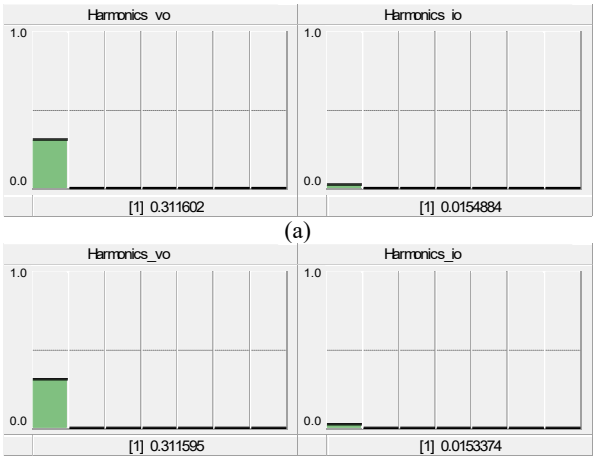

Fig. 13 The harmonic components: a) For conventional topology and b) For improved topology.

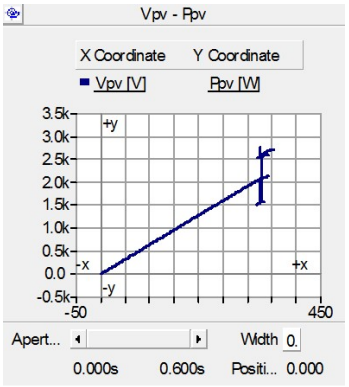

Fig. 14 Characteristic curve of PV panel voltage for improved topology in terms of PV panel power (V_{PV}–P_{PV}) under different circumstances of sun's radiations and temperatures.

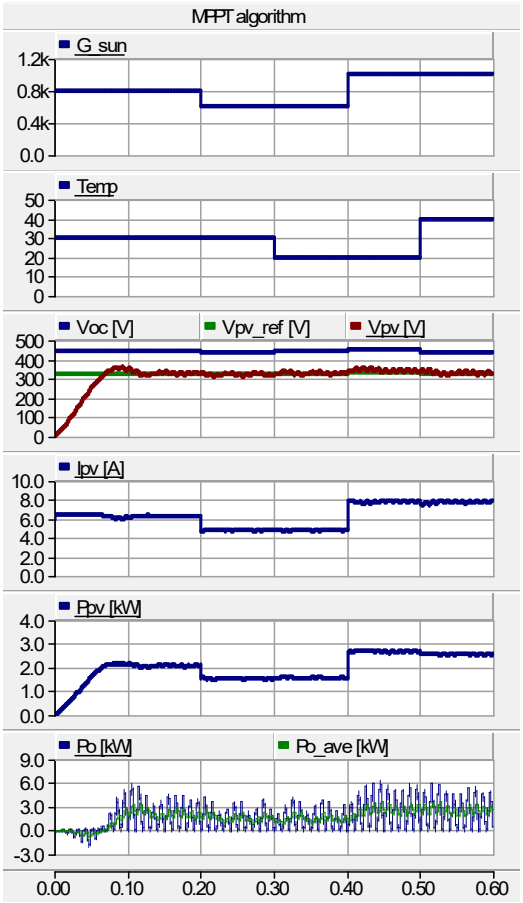

Fig. 15 Simulations results under different conditions of sun's radiations and temperatures for the improved H5 FB inverter included sun's radiations (G(W/m^2)), temperature (T(°C)), the voltage, current, and power of PV panel (V_{PV}, I_{PV}, and P_{PV}) and output power of inverter, respectively.

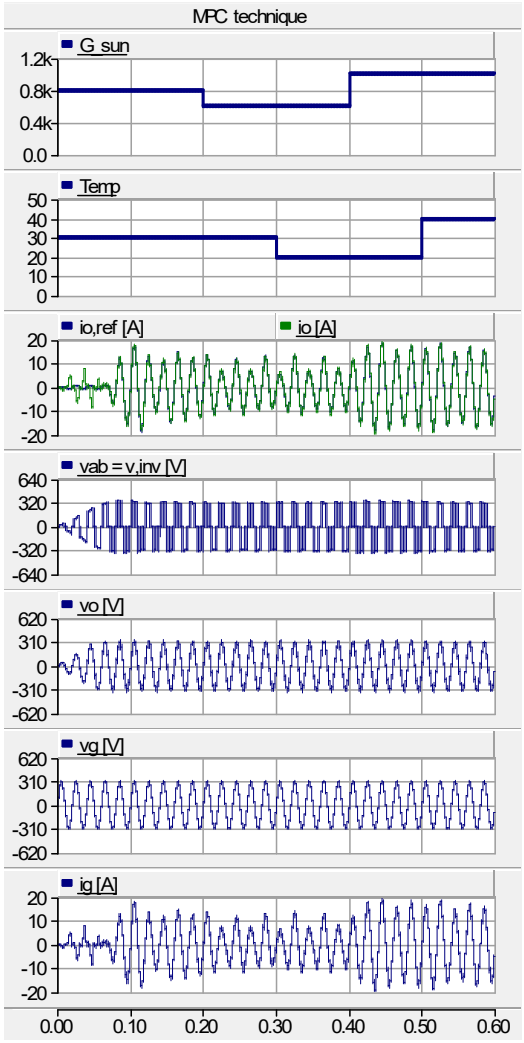

Fig. 16 Simulations results under different conditions of sun's radiations and temperatures for the improved H5 FB inverter included sun's radiations (G(W/m^2)), temperature (T(°C)), tracking of $i_{o,ref}$ by i_o, the output voltage of the inverter (v_{inv}), and the voltage across stabilizer capacitor (v_o), the voltage and current of grid (v_g and i_g), respectively.

current ($i_{o,ref}$) by the inverter output current (i_o). Fig. 16 illustrates tracking of $i_{o,ref}$ by i_o under different circumstances of weather for the improved H5 topology. It is clear that the reference current ($i_{o,ref}$) will alter due to the change in solar radiation and temperature. Considering Fig. 16, it is observed that the phase of the reference current is as same as the grid voltage phase. Hence, the reactive power injection into the grid will be approximately equal to zero ($Q \approx 0$). Fig. 16 proves the correct performance of the MPC controller under different circumstances of the sun's radiations and temperatures. As a result, the obtained simulation results confirm the good operation of the transformerless PV system based on the improved H5 FB inverter with the proposed control method by exploiting the FOCV and MPC strategies.

6 Conclusion

In this paper, several fundamental solutions which were simultaneously considered for a transformerless grid-connected PV system based on the improved H5 FB topology with the proposed control method by exploiting the FOCV and MPC techniques are respectively used for the more reduction of leakage current and switching losses, extraction of MPP and MPPT, and controlling the active and reactive powers. To prove the correct performance of the improved PV system with the proposed related controllers, the simulations were performed under different circumstances of sun radiations and temperatures. To confirm the operation of improved H5 FB inverter with the UPWM modulation technique, the simulation results indicated that the improved topology had been faultlessly reduced the ground leakage current. Moreover, to demonstrate that MPPT is exactly executed under different conditions of weather by using the proposed controller, the simulation results were exhibited. At last, to validate the suitable performance of the MPC controller for controlling the active and reactive powers, the simulation result was illustrated accurate tracking of the reference current ($i_{o,ref}$) by the inverter output current (i_o).

References

[1] B. Yang, W. Li, Y. Gu, W. Cui, and X. He, "Improved transformerless inverter with common-mode leakage current elimination for a photovoltaic grid-connected power system," *IEEE Transactions on Power Electronics*, Vol. 27, No. 2, pp. 752–762, Feb. 2012.

[2] W. Li, Y. Gu, H. Luo, W. Cui, X. He, and C. Xia, "Topology review and derivation methodology of single-phase transformerless photovoltaic inverters for leakage current suppression," *IEEE Transactions on Industrial Electronics*, Vol. 62, No. 7, pp. 4537–4551, Jul. 2015.

[3] X. Guo, R. He, J. Jian, Z. Lu, X. Sun, and J. M. Guerrero, "Leakage current elimination of four-leg inverter for transformerless three-phase PV systems," *IEEE Transactions on Power Electronics*, Vol. 31, No. 3, pp. 1841–1846, Mar. 2016.

[4] E. Amina and K. M. Shafeeque, "Single stage transformer less reconfigurable inverter for PV applications," in *International Conference on Inventive Research in Computing Applications (ICIRCA)*, pp. 388–392, 2018.

[5] Y. Zhu, J. Yao, and D. Wu, "Comparative study of two stages and single stage topologies for grid-tie photovoltaic generation by PSCAD/EMTDC," in *IEEE International Conference on Advanced Power System Automation and Protection*, Vol. 2, pp. 1304–1309, 2011.

[6] I. Anand, S. Senthilkumar, D. Biswas, and M. Kaliamoorthy, "Dynamic power management system employing a single-stage power converter for standalone solar PV applications," *IEEE Transactions on Power Electronics*, Vol. 33, No. 12, pp. 10352–10362, Dec. 2018.

[7] A. Moghadasi, A. Sargolzaei, A. Anzalchi, M. Moghaddami, A. Khalilnejad, and A. Sarwat, "A model predictive power control approach for a three-phase single-stage grid-tied PV module-integrated converter," *IEEE Transactions on Industry Applications*, Vol. 54, No. 2, pp. 1823–1831, Mar./Apr. 2018.

[8] J. W. Zapata, S. Kouro, G. Carrasco, H. Renaudineau, and T. A. Meynard, "Analysis of partial power DC–DC converters for two-stage photovoltaic systems," *IEEE Journal of Emerging and Selected Topics in Power Electronics*, Vol. 7, No. 1, pp. 591–603, Mar. 2019.

[9] J. Liu, S. Cheng, Y. Liu, and A. Shen, "FCS-MPC for a single-phase two-stage grid-connected PV inverter," *IET Power Electronics*, Vol. 12, No. 4, pp. 915–922, Oct. 2019.

[10] T. Kerekes, R. Teodorescu, P. Rodriguez, G. Vazquez, and E. Aldabas, "A new high-efficiency single-phase transformerless PV inverter topology," *IEEE Transactions on Industrial Electronics*, Vol. 58, No. 1, pp. 184–191, Jan. 2011.

[11] Y. Dai, W. Li, C. Zhou, and S. Zhuang, "Research on transformerless dual-buck full-bridge grid-connected inverter with H5-type for PV systems," *IET Power Electronics*, Vol. 12, No. 1, pp. 44–50, Dec. 2019.

[12] J. F. Ardashir, M. Sabahi, S. H. Hosseini, E. Babaei, and G. B. Gharehpetian, "A grid connected transformerless inverter and its model predictive control strategy with leakage current elimination capability," *Iranian Journal of Electrical and Electronic Engineering*, Vol. 13, No. 2, pp. 161–169, 2017.

[13] T. Ku, C. Chen, C. Lin, C. Hsu, and H. Chuang, "Transformer management system for energy control of customer demand response and PV systems," *IEEE Transactions on Industry Applications*, Vol. 55, No. 1, pp. 51–59, Jan./Feb. 2019.

[14] X. Guo, N. Wang, J. Zhang, B. Wang, and M. Nguyen, "A novel transformerless current source inverter for leakage current reduction," *IEEE Access*, Vol. 7, pp. 50681–50690, 2019.

[15] X. Guo, Y. Yang, R. He, B. Wang, and F. Blaabjerg, "Transformerless Z-source four-leg PV inverter with leakage current reduction," *IEEE Transactions on Power Electronics*, Vol. 34, No. 5, pp. 4343–4352, May 2019.

[16] A. K. Gupta, H. Agrawal, and V. Agarwal, "A novel three-phase transformerless H-8 topology with reduced leakage current for grid-tied solar PV applications," *IEEE Transactions on Industry Applications*, Vol. 55, No. 2, pp. 1765–1774, Mar./Apr. 2019.

[17] H. Li, Y. Zeng, B. Zhang, T. Q. Zheng, R. Hao, and Z. Yang, "An improved H5 topology with low common-mode current for transformerless PV grid-connected inverter," *IEEE Transactions on Power Electronics*, Vol. 34, No. 2, pp. 1254–1265, Feb. 2019.

[18] A. Das and G. Sheeja, "Photovoltaic H6-type transformerless inverter topology," in *IEEE Annual India Conference (INDICON)*, pp. 1–5, 2017.

[19] A. Das and G. Sheeja, "Photovoltaic H6-type transformerless inverter topology," in *IEEE Annual India Conference (INDICON)*, pp. 1–6, 2016.

[20] B. Ji, J. Wang, and J. Zhao, "High-efficiency single-phase transformerless PV H6 inverter with hybrid modulation method," *IEEE Transactions on Industry Applications*, Vol. 60, No. 5, pp. 2104–2115, May 2013.

[21] L. Zhang, K. Sun, Y. Xing, and M. Xing, "H6 transformerless full-bridge PV grid-tied inverters," *IEEE Transactions on Power Electronics*, Vol. 29, No. 3, pp. 1229–1238, Mar. 2014.

[22] F. Hasanzad, H. Rastegar, G. B. Gharehpetian, and M. Pichan, "Space vector modulation technique to reduce leakage current of a transformerless three-phase four-leg photovoltaic system," *Iranian Journal of Electrical and Electronic Engineering*, Vol. 13, No. 2, pp. 142–151, 2017.

[23] M. A. S. Masoum, H. Dehbonei, and E. F. Fuchs, "Theoretical and experimental analyses of photovoltaic systems with voltage- and current based maximum power-point tracking," *IEEE Transactions on Energy Conversion*, Vol. 17, pp. 514–522, Dec. 2002.

[24] T. Esram and P. L. Chapman, "Comparison of photovoltaic array maximum power point tracking techniques," *IEEE Transactions on Energy Conversion*, Vol. 22, No. 2, pp. 439–449, Jun. 2007.

[25] B. Subudhi and R. Pradhan, "A comparative study on maximum power point tracking techniques for photovoltaic power systems," *IEEE Transactions on Sustainable Energy*, Vol. 4, No. 1, pp. 89–98, Jan. 2013.

[26] Y. P. Huang, "A rapid maximum power measurement system for high-concentration photovoltaic modules using the fractional open-circuit voltage technique and controllable electronic load," *IEEE Journal of Photovoltaics*, Vol. 4, No. 6, pp. 1610–1617, Nov. 2014.

[27] M. Islam, S. Mekhilef, and M. Hasan, "Single phase transformerless inverter topologies for grid-tied photovoltaic system: A review," *Renewable and Sustainable Energy Rewiews*, Vol. 45, pp. 69–86, May 2015.

T. Ahmadzadeh was born in Tabriz, Iran, in 1986. He received the A.Sc. degree in Electronic Engineering from Islamic Azad University, Ahar Branch, Ahar, Iran, in 2006, the B.Sc. degree in Electronic Engineering from Islamic Azad University, Tabriz Branch, Tabriz, Iran, in 2009, and the M.Sc. degree in Electrical Engineering from the Aras International Campus, University of Tabriz, Tabriz, Iran, in 2014. He is currently working towards the Ph.D. degree in Electrical Engineering from the Department of Engineering, Shabestar Branch, Islamic Azad University, Shabestar, Iran. His current research interests include the analysis and control of power electronic converters and their applications.

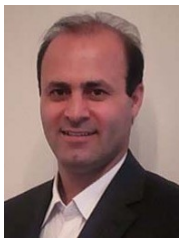

E. Babaei was born in Ahar, Iran, in 1970. He received the B.Sc. degree in Electronic Engineering and the M.Sc. degree in Electrical Engineering from the Department of Engineering, University of Tabriz, Tabriz, Iran, in 1992 and 2001, respectively, graduating with first class honors. He received the Ph.D. degree in Electrical Engineering from the Department of Electrical and Computer Engineering, University of Tabriz, in 2007. In 2004, he joined the Faculty of Electrical and Computer Engineering, University of Tabriz. He was an Assistant Professor from 2007 to 2011, an Associate Professor from 2011 to 2015, and has been Professor since 2015. He is the author of more than 300 journal and conference papers. He also holds 17 patents in the area of power electronics. His current research interests include the analysis and control of power electronic converters and their applications, dynamic power system, power system transients. Prof. Babaei has been the Editor-in-Chief of the Journal of Electrical Engineering of the University of Tabriz, since 2013. He is also currently an Associate Editor of the IEEE Transactions on Industrial Electronics. He is a Guest Editor for a special issue on "Recent Advances in Multilevel Inverters and their Applications" in the IEEE Transactions on Industrial Electronics. In 2013, he was the recipient of the Best Researcher Award from the University of Tabriz. Prof. Babaei has been included in the Top One Percent of the World's Scientists and Academics according to Thomson Reuters' list in 2015.

M. Sabahi was born in Tabriz, Iran, in 1968. He received the B.Sc. degree in electronic engineering from the University of Tabriz, the M.Sc. degree in electrical engineering from Tehran University, Tehran, Iran, and the Ph.D. degree in electrical engineering from the University of Tabriz, in 1991, 1994, and 2009, respectively. In 2009, he joined the Faculty of electrical and computer engineering, University of Tabriz, where he has been an associate professor since 2015. His current research interests include power electronic converters and renewable energy systems.

T. Abedinzadeh was born in Khoy, Iran, in 1983. He received the B.Sc. degree in Electrical Engineering from Iran University of Science and Technology, Tehran, Iran, in 2005, the M.Sc. degree in Electrical Engineering from Sharif University of Technology, Tehran, Iran, in 2007, and the Ph.D. degree in Electrical Engineering from Islamic Azad University, Science and Research Branch, Tehran, Iran, in 2014. He is a Faculty Member of Islamic Azad University-Shabestar Branch, Shabestar, Iran. His current research interests include power systems, smart grids, and renewable energies.